ISSN 0036-0295, Russian Metallurgy (Metally), Vol. 2020, No. 3, pp. 238–249. © Pleiades Publishing, Ltd., 2020.
Russian Text © The Author(s), 2020, published in Metally, 2020, No. 2, pp. 88–99.

Effect of a Pulsed Plasma Beam on the Structure and the Phase Composition of the Surface Layers in Ferritic–Martensitic Steels

I. V. Borovitskaya[a, *], V. N. Pimenov[a], V. A. Gribkov[a], N. A. Epifanov[a, b], S. A. Maslyaev[a], A. B. Mikhailova[a], G. G. Bondarenko[b], A. I. Gaidar[c], E. V. Demina[a], and M. D. Prusakova[a]

[a] *Baikov Institute of Metallurgy and Materials Science, Russian Academy of Sciences, Moscow, Russia*
[b] *Higher School of Economics, National Research University, Moscow, Russia*
[c] *Research Institute of Advanced Materials and Technologies, Moscow, Russia*
**e-mail: symp@imet.ac.ru*

Received April 16, 2019; revised June 24, 2019; accepted July 4, 2019

Abstract—The structure–phase changes that are caused in the surface layers of ferritic–martensitic Eurofer 97 and 10Cr9WV steel samples by the action of pulsed powerful fluxes of deuterium plasma and deuterium ions, which are generated in a plasma focus (PF) setup, are studied. Before tests, the steels were subjected to standard heat treatment (normalizing, tempering), and the 10Cr9WV steel samples were additionally annealed at 600°C for 600 h to determine the stability of the structure and properties at the temperatures that are close to the operating temperatures. During irradiation, the power densities of plasma ($q_{pl} = 10^7$–10^{10} W/cm^2) and ion ($q_i = 10^9$–10^{12} W/cm^2) fluxes and the number of plasma beam pulses (5–12 at a pulse duration of ~100 ns) are varied. The irradiation of the Eurofer 97 steel at $q_{pl} = 10^8$–10^{10} W/cm^2 in the PF setup is shown to cause melting and ultrafast solidification of the surface layer with the subsequent formation of a fine cellular structure with a cell size of 100–150 nm in it. The surface film formed on the 10Cr9WV steel samples during preliminary long-term annealing is found to begin to fail at $q_{pl} = 10^8$ W/cm^2; this film is fully removed at $q_{pl} = 10^{10}$ W/cm^2. This process is accompanied by the segregation of particles 1–3 μm in size, which are enriched in manganese, chromium, and oxygen. After the surface film is removed, irradiation promotes the removal of manganese from the surface layers, and manganese is also removed from the Eurofer 97 steel, which has no surface film in the initial state. The plasma beam treatment of the Eurofer 97 steel in the PF working chamber at $q_{pl} = 10^8$ W/cm^2 is found to cause the formation of retained austenite in its structure, and the content of retained austenite in the 10Cr9WV steel subjected to similar treatment is lower than in the Eurofer 97 steel by a factor of 20 because of the presence of a film on its surface. The irradiation of the 10Cr9WV steel at a higher power density ($q_{pl} = 10^{10}$ W/cm^2), when the surface film is removed, equalizes the contents of retained austenite in the steels under study.

Keywords: pulsed plasma, plasma focus setup, ferritic–martensitic steel, Eurofer 97 steel, 10Cr9WV steel, structure–phase changes, surface

DOI: 10.1134/S0036029520030027

INTRODUCTION

Ferritic and ferritic–martensitic steels are now considered as advanced structural materials for nuclear and thermonuclear reactors (TNRs) [1–5]. Their advantages over austenitic steels are a low level of irradiation-induced swelling, a high thermal conductivity, and a low thermal expansion coefficient [6]. These materials are known to undergo pulsed thermal, radiation, and mechanical loads [7]; therefore, it is important to estimate their resistance to these extreme actions.

Plasma focus (PF) setups are effective to model the TNR operating conditions [8–10]. The parameters of the pulsed plasma and fast ion fluxes generated in these setups are close to those during the interaction of ionizing radiation with the materials facing plasma in the working chambers of controlled nuclear synthesis plants with inertial and magnetic plasma confinement. High flux power densities (10^7–10^{12} W/cm^2) are reached in one pulsed PF discharge with the pulse duration of hot plasma (temperature up to 1 keV), fast electrons and ions (with an energy of 0.1–1.0 MeV), and X-ray and neutron radiation in the range 10^{-8}–10^{-6} s.

Table 1. Chemical compositions, wt %, of the steels under study (Fe base)

Steel grade	C	Cr	Mn	W	V	Ta	N	P	Si	S
Eurofer 97	0.11	9.0	0.48	1.1	0.20	0.07	0.03	0.005	–	–
10Cr9WV	0.11	9.2	0.65	1.0	0.15	0.10	0.03	0.020	0.3	0.007

The purpose of this work is to study the influence of the pulsed plasma beam created in the working chamber of PF on the structure and the phase and elemental compositions of the surface layers in ferritic–martensitic steels.

EXPERIMENTAL

We investigated samples of ferritic–martensitic Eurofer 97 steel developed in Europe and 10Cr9WV steel developed in Russia (Table 1). The Eurofer 97 steel samples in the initial state were subjected to final heat treatment (HT) under the following conditions: normalizing at 980°C, 30 min + tempering at 760°C, 90 min. Apart from standard HT (normalizing at 1050°C, 30 min + tempering at 780°C, 1 h), the 10Cr9WV steel samples were additionally annealed at 600°C for 600 h in sealed ampules and were then air cooled to determine the stability of the structure and properties at the temperatures that are close to the operating temperatures.

The samples were irradiated by pulsed high-temperature plasma and ion fluxes on a PF-6 setup (Poland) [11]. The setup generated 2-kJ fluxes, the particle density in a plasma flow was ~10^{18} cm^{-3}, the plasma flow speed was ~10^7 cm/s, the plasma pulse duration was 100 ns, and the fast-ion pulse duration was 20 ns. Deuterium at a pressure p = 6.4 Torr was used a working gas. The irradiation conditions are given in Table 2.

The samples to be irradiated were located along the axis of the working chamber normal to the incident energy flux at a distance l = 4.3–18.3 cm from the setup anode. The number of pulsed discharges was changed from N = 5 to 12 with an interpulse interval of ~3 min. The radiation–thermal action intensity changed correspondingly: the plasma power density changed in the range 10^7–10^{10} W/cm^2, and the ion flux power density changed in the range 10^9–10^{12} W/cm^2 (see Table 2).

After irradiation, the samples were analyzed using an EVO 40 (Carl Zeiss) scanning electron microscope equipped with an electron-probe microanalysis (EPMA) attachment. X-ray diffraction (XRD) analysis was carried out on an Ultima IV (Rigaku, Japan) diffractometer using Cu $K\alpha$ radiation in the angular range $2\theta = 9°$–$125°$. The phase analysis of the samples was performed using the PDXL software package and the ICDD database.

The changes in the surface layer temperature were estimated by numerical simulation using the one-dimensional model from [12]. In the calculation, the plasma power density was taken to be $q_{pl} = 10^8$ W/cm^2, the plasma action time was τ_{pl} = 100 ns, the ion flux power density was $q_i = 10^{10}$ W/cm^2, the action time was τ_i = 20 ns, and the secondary-plasma parameters were $q_{sp} = 10^6$ W/cm^2 and τ_{sp} = 1 μs.

RESULTS AND DISCUSSION

Eurofer 97 Steel

Figures 1–3 show the surface microstructure of the Eurofer 97 steel samples after irradiation at a various plasma and ion flux power densities.

Irradiation did not melt the surface layer at the maximum distance from a target sample to the anode unit of the setup (Table 2, regime I). Only circular planar copper drops appear on the sample surface as a result of copper evaporation by an electron beam from the copper anode and copper deposition on the sample surface (Fig. 1a, spectrum in Fig. 1b) [10]. Spherical particles ~300 nm in size, which consist of complex tantalum-based carbonitrides and were present in the initial samples, are retained in the structure of the material (Fig. 1c, Table 3). Copper in the spectrum of particles deposited onto the target surface is also present in the composition of the surface layer over the entire irradiated surface (Figs. 1a, 1b). The X-ray diffraction patterns of the samples irradiated according to regime I also have no substantial changes.

The samples located at smaller distances from the anode, namely, l = 13.8 and 4.3 cm (Table 2; regimes II and III, respectively), undergo more significant changes.

Table 2. Steel sample irradiation conditions in a PF-6 setup

Steel sample	Regime	l, cm	N	q_{pl}	q_i
				W/cm^2	
Eurofer 97	I	18.3	7	10^7	10^9
	II	13.8	7	10^8	10^{10}
	III	4.3	12	10^{10}	10^{12}
10Cr9WV	I	18.3	5	10^7	10^9
	II	13.8	9	10^8	10^{10}
	III	4.3	6	10^{10}	10^{12}

l is the distance from the anode; N is the number of pulses; and q_{pl} and q_i are the plasma and ion flux power densities, respectively.

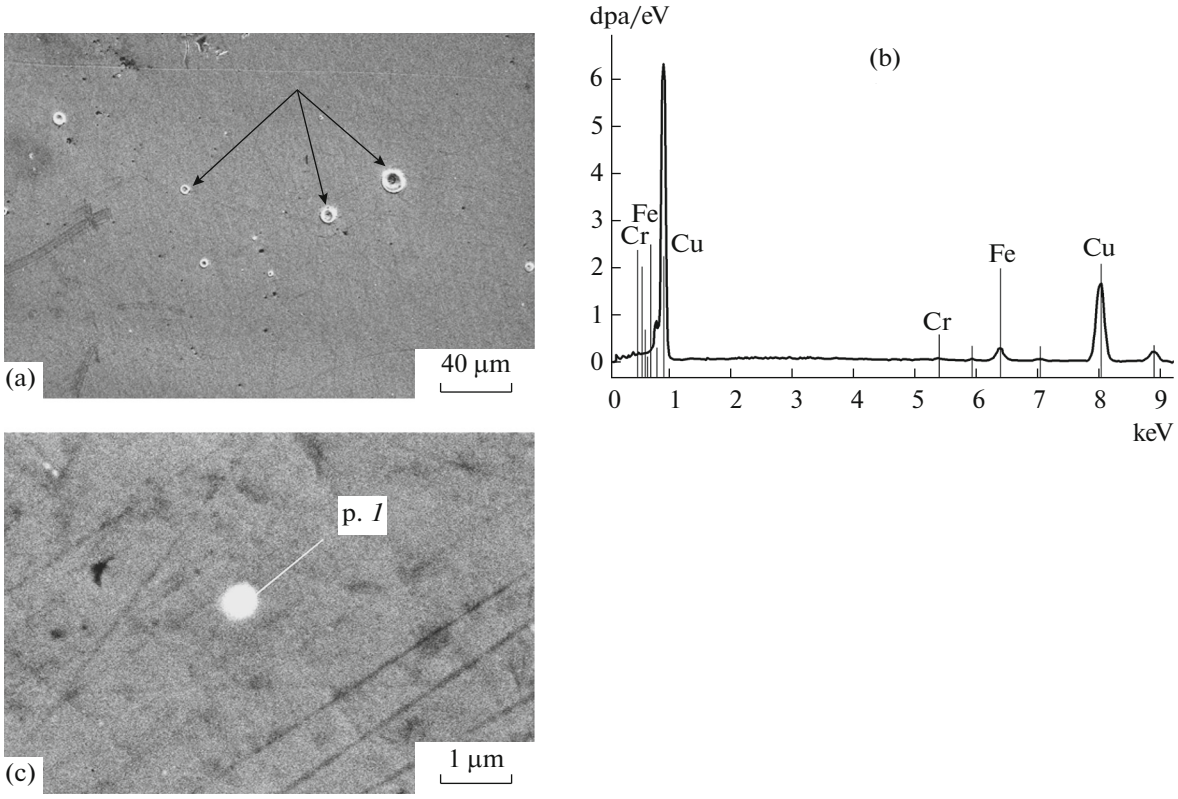

Fig. 1. (a) Surface structure of Eurofer 97 steel after irradiation in the PF setup at a distance of 18.3 cm from the anode. The irradiation power density is $q_{pl} = 10^7$ W/cm^2 and $q_i = 10^9$ W/cm^2. The arrows indicate copper drops deposited from the PF setup anode. (b) Spectrum of the copper drops. (c) Point *1*, oxycarbonitride particle (its composition is given in Table 3).

Figure 2 shows the microstructure of the samples irradiated at $l = 13.8$ cm ($q_{pl} = 10^8$, $q_i = 10^{10}$ W/cm^2). The surface is seen to be melted by irradiation and it acquires a wavy relief (Fig. 2a). The microstructure has regions with a martensite structure, especially at wave crests (Figs. 2b, 2c). EPMA demonstrates that the chemical composition of the surface layers changed weakly (Table 4). The surface layer is depleted of manganese, which tends toward evaporation at high temperatures because of a high vapor pressure, and copper is deposited from the anode unit of the PF setup.

It should be noted that the predominant evaporation of manganese from the surface layer was also observed during the pulsed action of helium ion fluxes on plane-parallel samples of austenitic chromium–manganese Cr12Mn14Ni4 (Al, Mo) steel [13], the action of hydrogen ions and hydrogen plasma on plane-parallel samples of austenitic chromium–manganese 10Cr12Mn20W steel, and the deuterium plasma beam irradiation of a hexagonal tube made of this steel [14, 15].

The X-ray diffraction patterns recorded after irradiation contain significantly broadened (310) lines of the α phase (Fig. 4c), which can indirectly indicate an increase in the lattice tetragonality (because of the presence of martensite in the alloy composition). However, the broadening of XRD peaks after plasma beam treatment of metallic materials was also detected in other investigations and can be related to the appearance of numerous defects, lattice microdefor-

Table 3. Chemical compositions of the complex oxycarbonitride phases that are present in the Eurofer 97 steel (Fig. 1c, point *1*)

Sample	Element content in particle, at %								
	Fe	Ta	Cr	Mn	Ti	V	C	N	Cu
Initial	20.15	21.65	2.97	1.56	1.37	0.75	35.73	14.39	–
Irradiated according to regime I	15.26	13.14	2.45	–	1.70	0.49	47.00	18.14	1.82

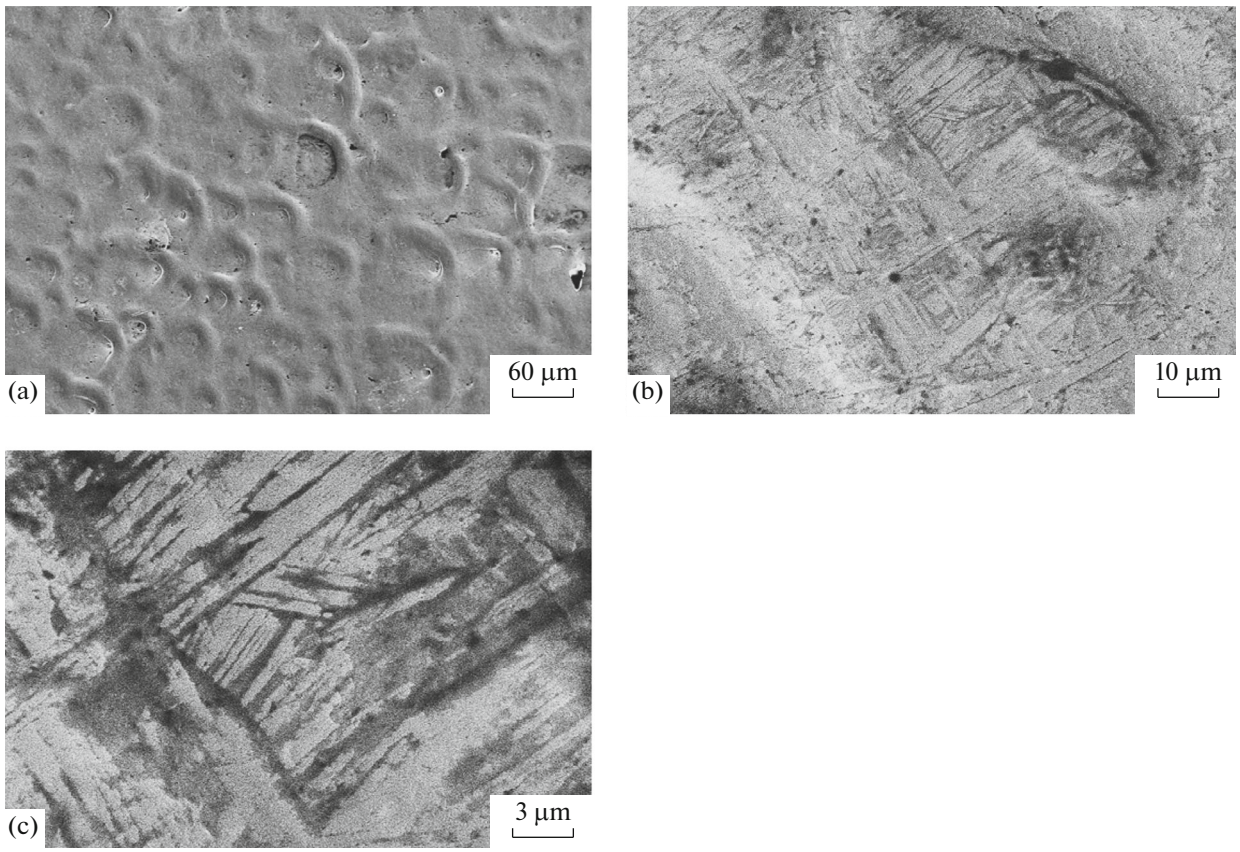

Fig. 2. (a–c) Surface microstructure of the Eurofer 97 steel at various magnifications after irradiation in the PF setup at a distance of 13.8 cm from the anode ($q_{pl} = 10^8$ W/cm^2, $q_i = 10^{10}$ W/cm^2).

mation, and a decrease in the coherent domain size in the surface layer of the metal subjected to PF treatment [16]. As a result, X rays are diffracted in an angular range $\theta \pm \Delta\theta$, and diffraction peaks are broadened when the plasma action power increases.

In addition, clear (111), (200), and (220) lines of γ austenite appear in X-ray diffraction patterns. Therefore, austenite forms during PF treatment according to regime II in the course of recrystallization, and it is partly retained upon cooling. A similar phase transformation effect was observed when Eurofer 97 steel samples were irradiated in a PF-1000 setup by hydrogen ion fluxes and hydrogen plasma [17]. This effect was most pronounced at a high irradiation power density ($q \approx 10^{10}$ W/cm^2), as in this work. In deeper layers (where melting was not reached), austenite can also appear due to the $\alpha \rightarrow \gamma$ transformation in heating. According to thermal calculations (Fig. 5), the melted layer thickness after the action of one energy pulse was ~0.8 μm, and the temperature in the surface layer 1.5–2 μm thick increased to 600–800°C. This increase in the temperature in combination with a shock wave, which always accompanies a plasma beam action at $q \geq 10^{10}$ W/cm^2 and generates point and

Table 4. Chemical compositions, at %, of the surface layers in the Eurofer 97 steel irradiated under various conditions

Regime	Fe	Cr	Mn	W	V	N	C**	Cu
Ini.*	78.65	8.07	0.34	0.20	0.13	–	12.60	–
II	72.67	7.60	–	0.11	–	8.12	10.88	0.62
III	66.45	6.25	–	0.15	–	8.21	16.46	2.49

* Initial state.

** The carbon content is overestimated because of the polymerization of hydrocarbons adsorbed on the sample surface under an electron probe.

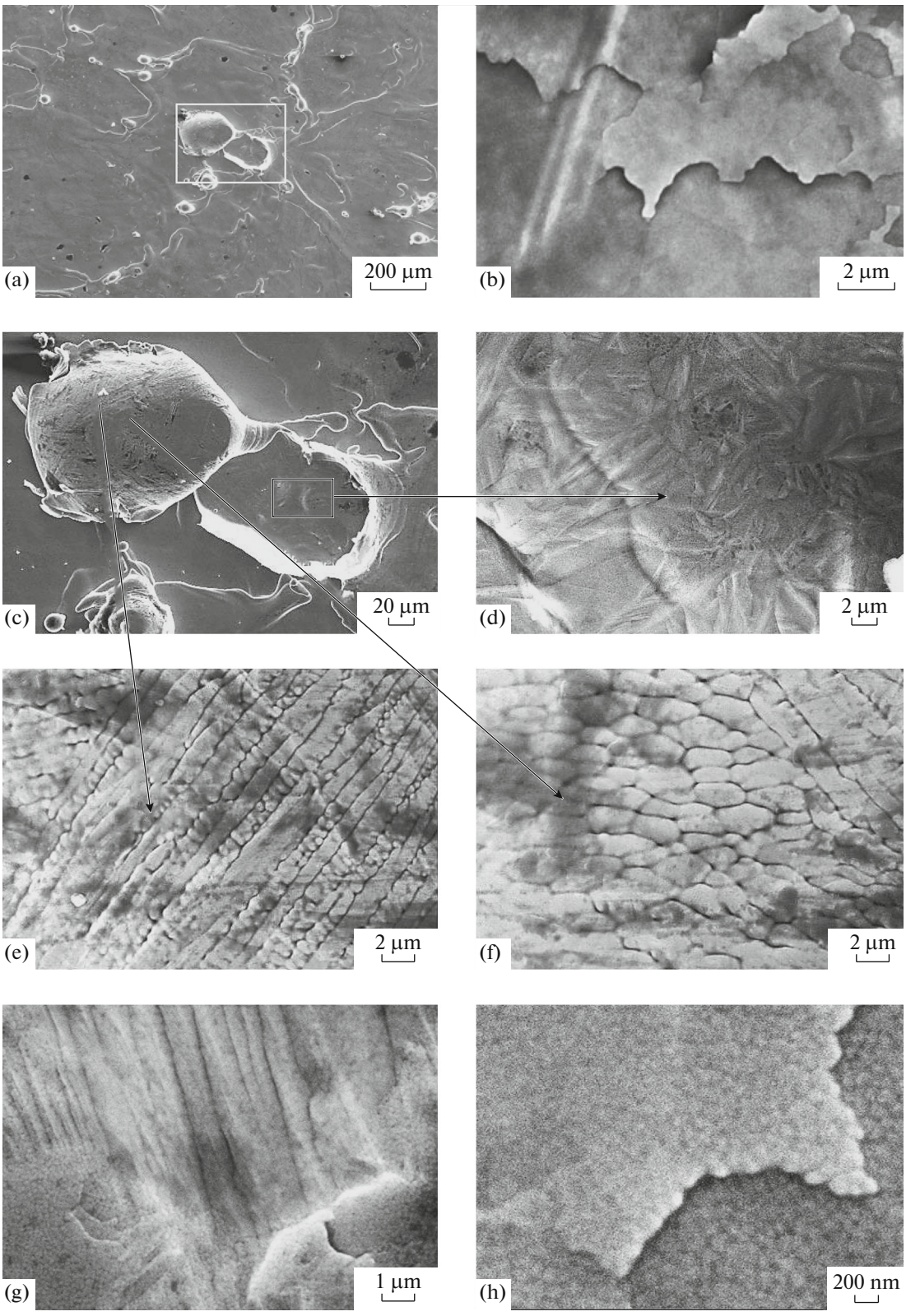

Fig. 3. Microstructures of some surface regions ((a, b, g) general view at various magnifications) in the Eurofer 97 steel subjected to irradiation in the PF setup at a distance of 4.3 cm from its anode. The radiation power density is $q_{pl} = 10^{10}$ W/cm^2 and $q_i = 10^{12}$ W/cm^2. (c) Solidified melt drop at a wave crest (indicated by the rectangle in (a)). (d–f) The types of microstructure in the region indicated in (c). (h) Fine cellular structure of the surface layer revealed at a high magnification.

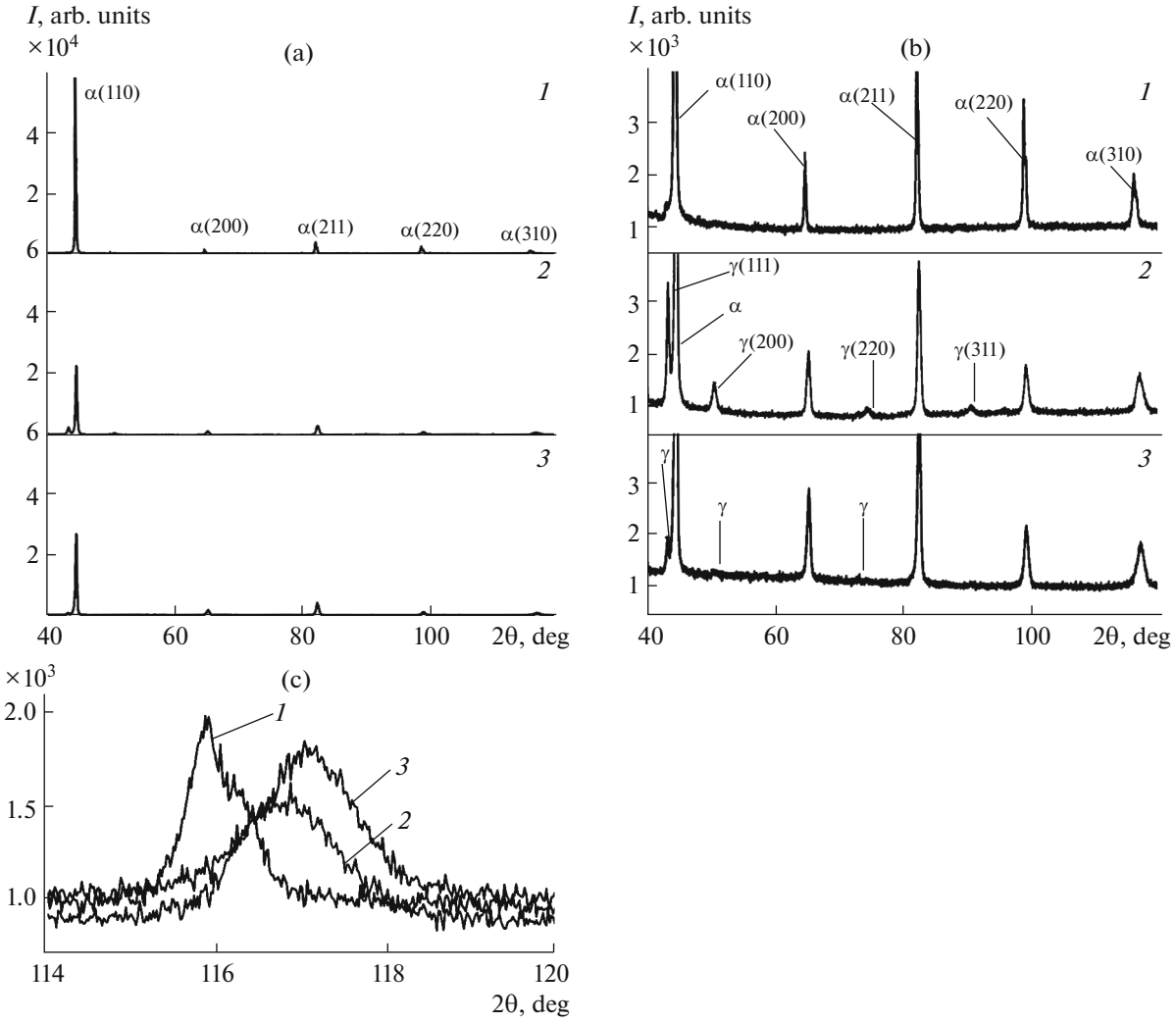

Fig. 4. X-ray diffraction patterns of Eurofer 97 steel samples (regions *1* in (a, b)) in the initial state and after irradiation in the PF setup at (regions *2* in (a, b)) $l = 13.8$ cm and (regions *3* in (a, b)) $l = 4.3$ cm. (b) Refining of the X-ray diffraction patterns in (a) in the range of low-intensity lines. (c) Refining of the X-ray diffraction patterns shown in (a) in the angular range $2\theta = 114–120$ deg.

linear defects in the target volume [18], promotes the diffusion mass transfer of the alloy components and the phase transformation.

At the minimum distance from the anode (l = 4.3 cm), the melted surface has a wavy relief, which differs from the relief formed upon irradiation at a longer distance from the anode (13.8 cm; cf. Figs. 2a and 3a). The wave crests contain bulges in the form of solidified melt drops, which were observed earlier after the treatment of various metals by pulsed high-energy fluxes [16, 19]. As was shown in [20], this wavy relief is caused by the following two factors: plasma pressure and the reactive action of vapor fluxes from the surface layer of the molten metal.

Figures 3c–3f show photographs of the various types of microstructure formed near one of the bulges in the zone indicated in Fig. 3a, where a hollow bulge moved and detached (detachment and motion were likely to be caused by gas release in this zone; this phenomenon was comprehensively described in [14]). The edges of the displaced dome are thin and curved up, and a crater with a martensitic structure at the bottom formed at the detachment site (Fig. 3d). Recrystallization inside the former martensite lamellae with the formation of equiaxed 1-μm grains took place in the separated part (dome; Figs. 3e, 3f). Thus, regions having different structure–phase states adjoin each other at the surface due to a nonuniform temperature distribution over the irradiated surface, since the phase composition and the microstructure of the steels are substantially determined by the temperature and the cooling rate.

On the whole, the surface of the Eurofer 97 steel samples irradiated under the experimental conditions has a cellular structure with a cell size of 100–150 nm (Fig. 3h). The formation of a fine cellular structure is characteristic of ultrahigh cooling rates in a molten surface layer, which can be reached during, e.g., laser

or plasma surface treatment. The character of structure during solidification is known to depend on the ratio of the nucleation and growth rates, which depend on the supercooling of the melt (which increases with the cooling rate) [21]. When the supercooling is high, the linear rate of crystal growth decreases significantly, which prevents dendritic growth and favors the formation of a fine cellular structure.

The X-ray diffraction patterns of the samples irradiated according to regime III point to the appearance of a ultimate strength in the structure (Fig. 4a, region *3*), and its amount is smaller than that formed after treatment according to regime II (Table 5). This difference can be due to the following: at a very high power density ($q_{pl} = 10^{10}$, $q_i = 10^{12}$ W/cm^2), a significant part of the irradiated surface layer evaporates, and the radiation-modified surface layer thickness decreases correspondingly.

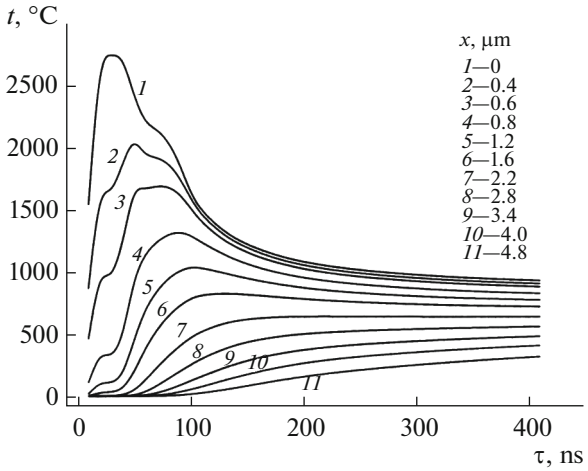

Fig. 5. Time t variation of the Eurofer 97 steel sample temperature t at distance x from the irradiated surface. The irradiation parameters are as follows: one plasma and fast ion flux pulse at a distance of 13.8 cm from the anode to the surface to be irradiated, the adsorbed plasma power density is $q_{pl} = 10^8$ W/cm^2, the plasma pulse duration is 100 ns, the adsorbed power density of a fast ion flux is $q_i = 10^{10}$ W/cm^2, and the fast deuteron pulse duration is 20 ns.

Table 5. Austenite content, wt %, in the surface layers of the Eurofer 97 and 10Cr9WV steel samples subjected to treatment in the PF setup

Regime	Eurofer 97	10Cr9WV
Initial	Undet	Undet
II	14.6	0.6
III	1.3	1.3

10Cr9WV Steel

The surface of the samples subjected to long-term annealing in a pumped out sealed ampule at 600°C for 600 h is coated with a black film, which consist of the product of interaction of the alloy components with the residual gases in the ampule. Microstructural analysis demonstrates that the surface has many 1-μm particles (Fig. 6a), most of which are faceted (Fig. 6b). As follows from EPMA data (Table 6), the particle composition is close to the composition of the environment, and the particles are often enriched in a certain alloy component (Cr, Si, W, Mn, Fe). Despite the continuous film, the structure has approximately equiaxed ferrite grains (film along grain boundaries is likely to be thinner).

The samples were irradiated without removing the surface film in order to estimate the stability of the film under the plasma beam treatment conditions and how the film can protect the base metal against melting and structure–phase changes. After irradiation at the minimum power density ($q_{pl} = 10^7$ W/cm^2, $l = 18.3$ cm), the film is retained and cracks appear in some regions. The particles become more spherical without clear facets: they are likely to be partly melted during plasma treatment (Fig. 7).

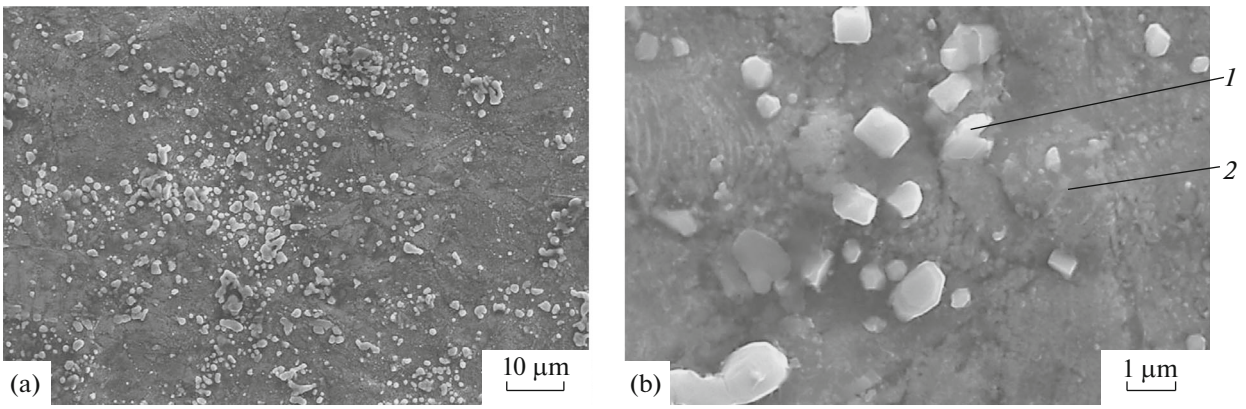

Fig. 6. Surface microstructure of the 10Cr9WV steel subjected to long-term annealing at 600°C for 600 h: (a) general particle distribution and (b) morphology of particles (some faceted particles are visible).

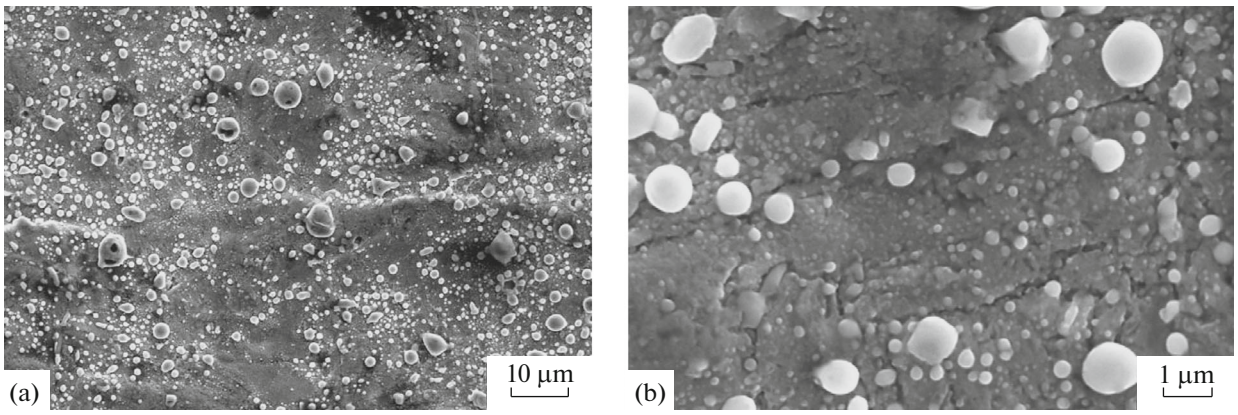

Fig. 7. Surface microstructure of the 10Cr9WV steel subjected to long-term annealing at 600°C for 600 h and irradiation in the PF setup at a distance of 18.3 cm from the anode and a radiation power density $q_{pl} = 10^7$ W/cm^2 and $q_i = 10^9$ W/cm^2: (a) general particle distribution and (b) morphology of particles (spherical) at a magnification higher than in (a).

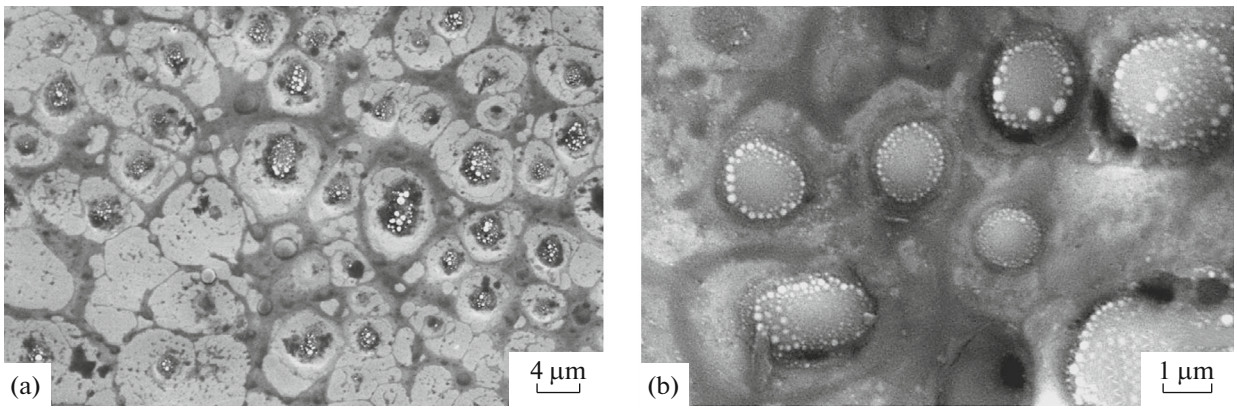

Fig. 8. Surface microstructure of the 10Cr9WV steel subjected to long-term annealing at 600°C for 600 h and irradiation in the PF setup at a distance of 13.8 cm from the anode and a radiation power density $q_{pl} = 10^8$ W/cm^2 and $q_i = 10^{10}$ W/cm^2: (a) structure refinement film on the steel surface and (b) film fragment at a magnification higher than in (a). Spherical particles are visible on the film surface.

When the treatment power density increases to $q_{pl} = 10^8$ W/cm^2 (l = 13.8 cm), the surface film begins to fail and irregular cells begin to form. Small film fragments form spherical particles due to surface tension forces and are arranged near failure regions (Fig. 8). Defects in the form of craters, i.e., through failure sites, also exist. EPMA data demonstrate that the average element contents at the surface after treatment according to this regime change slightly (Table 7): the oxygen content decreases because of the failure of the surface film, the manganese content decreases slightly, and copper is deposited from the anode onto the sample surface. Copper is uniformly distributed over the surface and is also deposited in the form of flat drops.

Although the average element contents in the surface layer change weakly after irradiation according to regime II (Table 7), the failure of the film is accompanied by the segregation of manganese and chromium in the form of individual particles and film fragments, which also contain oxygen (Fig. 9, point *4*). In addition, the structure contains spherical particles

Table 6. Elemental compositions of the surface layers in the 10Cr9WV steel subjected to long-term annealing at 600°C for 600 h (analysis of particle *1* and particle-free surface *2* (see Fig. 6b))

Analysis region	Element content, at %								
	Fe	Cr	Mn	W	V	Si	Al	C	O
1	76.53	4.69	1.21	–	–	0.16	0.10	16.53	0.77
2	74.20	5.08	–	0.17	0.06	0.42	0.08	18.13	1.85

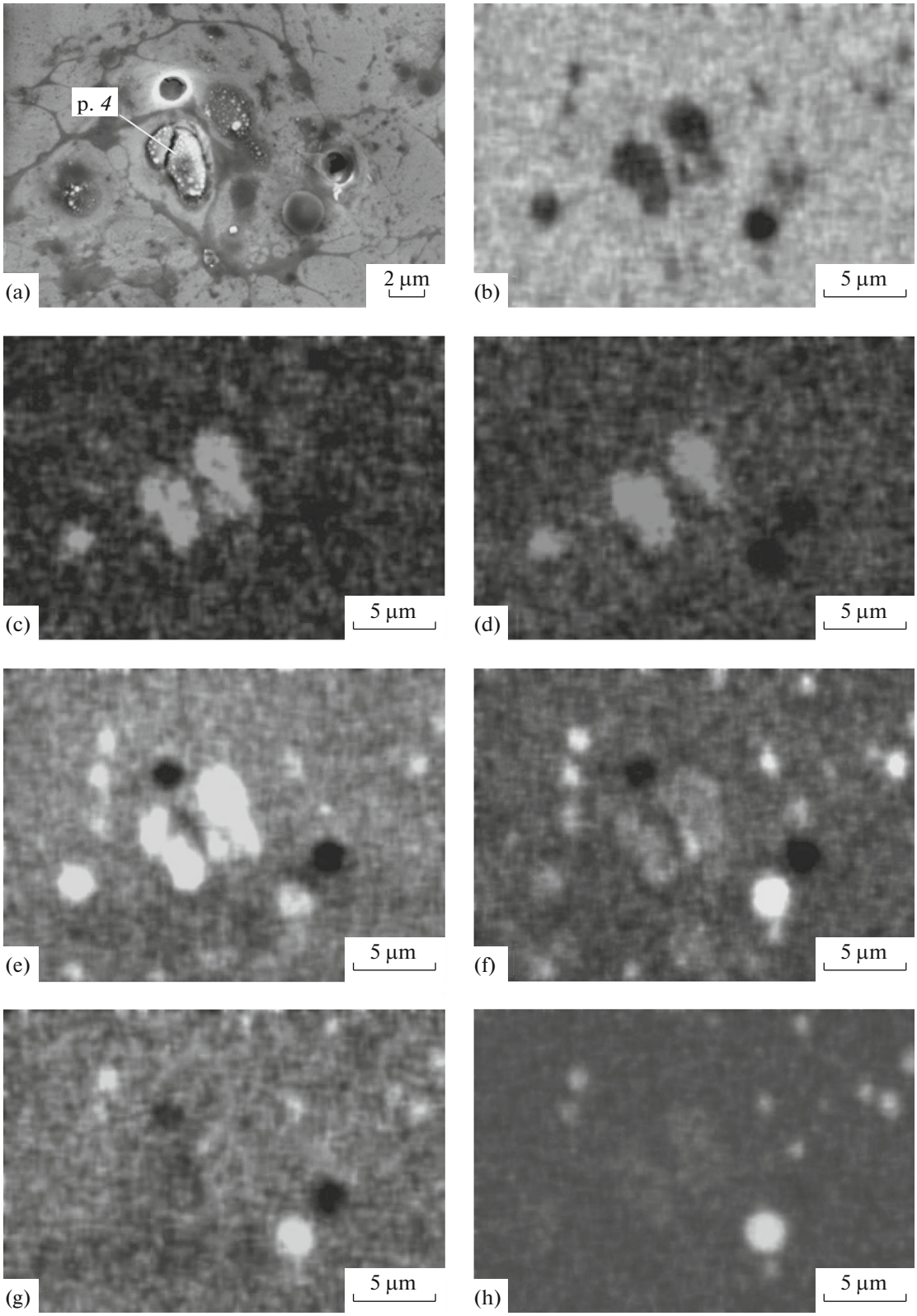

Fig. 9. Surface microstructure of the 10Cr9WV steel subjected to long-term annealing at 600°C for 600 h and irradiation in the PF setup at a distance of 13.8 cm from the anode and $q_{pl} = 10^8$ W/cm^2 and $q_i = 10^{10}$ W/cm^2: (a) secondary electrons and characteristic X-ray radiation of (b) Fe, (c) Mn, (d) Cr, (e) O, (f) Si, (g) Al, (h) Ca.

Table 7. Average chemical compositions, at %, of the surface layers in the 10Cr9WV steel subjected to irradiation under various conditions

Regime	Fe	Cr	Mn	W	V	Si	Al	C	O	Cu
Ini*	59.78	5.43	2.38	0.27	0.14	0.16	0.12	22.35	9.36	–
II	72.64	6.01	1.76	0.17	0.12	0.35	0.02	16.87	0.49	1.57
III	68.59	6.83	Undet	0.46	0.08	0.35	0.29	19.61	–	3.81

* Initial state.

enriched in the elements entering in the compositions of the structural and functional components of the PF working chamber (Fig. 9; O, Si, Al, Ca).

When the samples are irradiated at the smallest distance from the anode ($l = 4.3$ cm, $q_{pl} = 10^{10}$ W/cm^2), the surface layer is melted and the topography of the appearing wavy relief is close to that of the Eurofer 97 steel irradiated under similar conditions (Figs. 10a, 3a). The microstructure of the surface layer has craters caused by gas release (Fig. 10b). The surface film is removed during irradiation and the manganese content decreases sharply (see Table 7). Moreover, the microstructure mainly has many ferrite grains (see Fig. 10c) and some regions with a martensitic structure (Fig. 10d).

XRD analysis showed that the content of retained austenite is low (Table 5; 0.6 wt % for 10Cr9WV steel and regime II, 14.6 wt % for Eurofer 97 steel) after irradiation at a low power density (regimes I, II), when the surface film is retained and the base metal under it

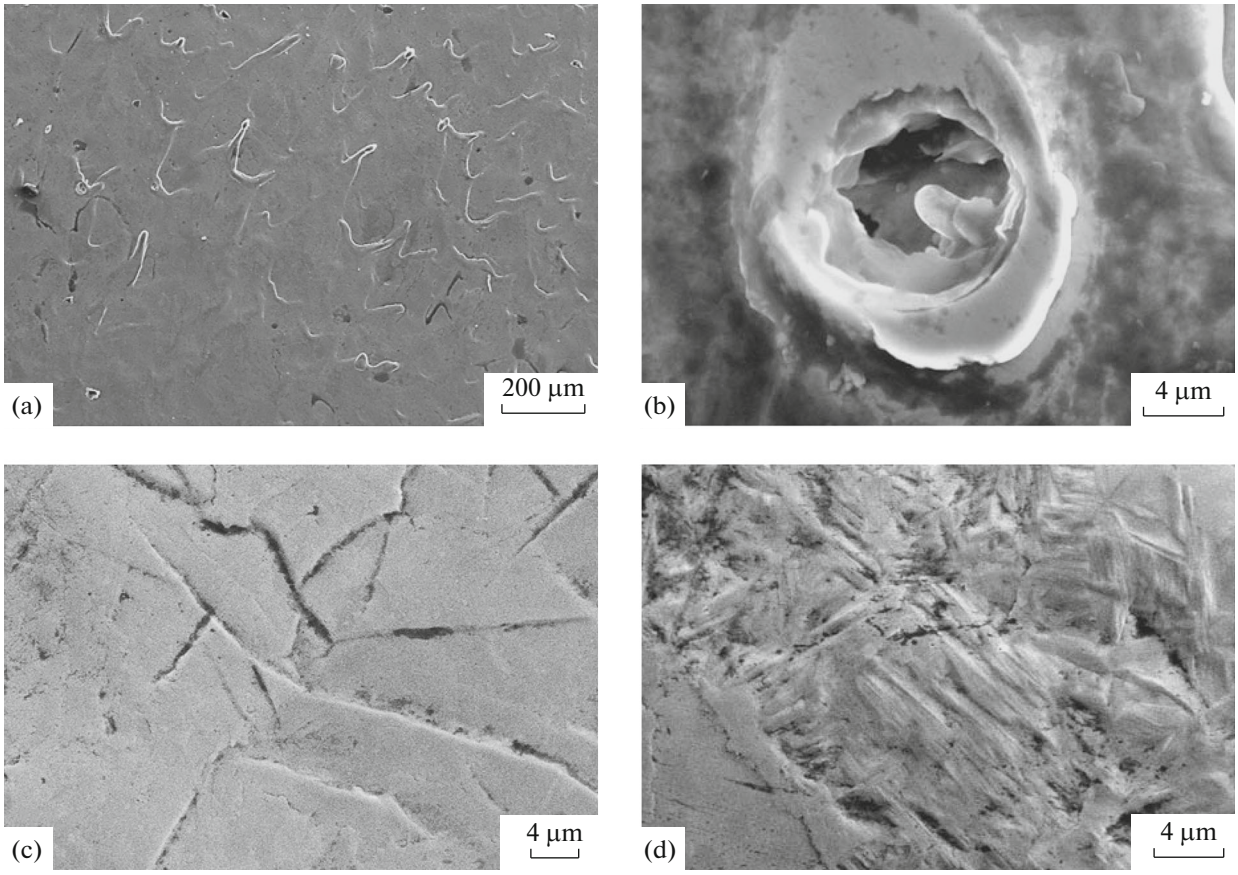

Fig. 10. Surface microstructure of the 10Cr9WV steel subjected to long-term annealing at 600°C for 600 h and irradiation in the PF setup at a distance of 4.3 cm from the anode and $q_{pl} = 10^8$ W/cm^2 and $q_i = 10^{10}$ W/cm^2: (a) general view of the surface, (b) crater formed during gas release, (c) region with ferritic structure, and (d) region with martensitic structure.

does not melt. After the surface film is removed (regime III), the content of retained austenite is similar to that in the Eurofer 97 steel irradiated under the same conditions (Table 5, 1.3 wt %).

CONCLUSIONS

(1) We studied the influence of pulsed powerful fluxes of deuterium plasma and deuterium ions generated by the PF setup (plasma flux power density is $q_{pl} = 10^7$–10^{10} W/cm^2, ion power density is $q_i = 10^9$–10^{12} W/cm^2) on the structure–phase changes in the surface layers of ferritic–martensitic steels, namely, Eurofer 97 steel subjected to standard HT and 10Cr9WV steel subjected to additional annealing at 600°C for 600 h. The irradiation of the Eurofer 97 steel at $q_{pl} = 10^8$–10^{10} W/cm^2 was shown to cause melting and ultrafast solidification of the surface layer with the subsequent formation of a fine cellular structure with a cell size of 100–150 nm. The surface film formed on the 10Cr9WV steel during preliminary long-term annealing was found to begin to fail at $q_{pl} = 10^8$ W/cm^2; this film was fully removed at $q_{pl} = 10^{10}$ W/cm^2. This process is accompanied by the segregation of particles 1–3 μm in size, which are enriched in manganese, chromium, and oxygen. After the surface film was removed, irradiation promoted the removal of manganese from the surface layers, and manganese was also removed from the Eurofer 97 steel, which had no surface film in the initial state.

(2) The plasma beam treatment of the Eurofer 97 steel in the PF working chamber at $q_{pl} = 10^8$ W/cm^2 was found to cause the formation of retained austenite, and the content of retained austenite in the 10Cr9WV steel subjected to similar treatment was lower than in the Eurofer 97 steel by a factor of 20 because of the presence of a film on its surface. The irradiation of the 10Cr9WV steel at a higher power density ($q_{pl} = 10^{10}$ W/cm^2), when the surface film was removed, equalized the contents of retained austenite in the steels under study.

FUNDING

This work was performed in terms of state assignment no. 075-00746-19-00.

REFERENCES

1. R. L. Klueh and A. T. Nelson, "Ferritic/martensitic steels for next-generation reactors," J. Nucl. Mater. **371**, 37–52 (2007).
2. Y. Li, Q. Huang, Y. Wu, T. Nagasaka, and T. Muroga, "Mechanical properties and microstructures of China low activation martensitic steel compared with JLF-1," J. Nucl. Mater. **367–370**, 117–121 (2007).
3. S. V. Rogozhkin, V. S. Ageev, A. A. Aleev, A. G. Zaluzhnyi, M. V. Leont'eva-Smirnova, and A. A. Nikitin, "Tomographic atom-probe analysis of temperature-resistant 12%-chromium ferrite–martensite steel EK-181," Fiz. Met. Metalloved. **108** (6), 612–618 (2009).
4. N. A. Polekhina, I. Yu. Litovchenko, K. V. Almaeva, A. N. Tyumentsev, Yu. P. Pinzhin, V. M. Chernov, and M. V. Leont'eva-Smirnova, "Comparative investigation of the microstructures, the mechanical properties, and the fractures of high-temperature martensitic steels EK-181, ChS-139, and EP 823 in the temperature range from –196 to 720°C," VANT, Ser. Termoyad. Sintez **41** (4), 38–47 (2018).
5. Q. Huang, N. Baluc, Y. Dai, S. Jitsukawa, A. Kimura, J. Konys, R. J. Kurtz, R. Lindau, T. Muroga, G. R. Odette, B. Raj, R. E. Stoller, L. Tan, H. Tanigawa, A.-A. F. Tavassoli, T. Yamamoto, F. Wan, and Y. Wu, "Recent progress of R&D activities on reduced activation ferritic/martensitic steels," J. Nucl. Mater. **442**, S2–S8 (2013).
6. T. N. Kompaniets, "Choice of steels for DEMO reactor," VANT, Ser. Termoyad. Sintez, No. 3, 16–24 (2009).
7. B. I. Khripunov, V. B. Petrov, S. N. Kornienko, A. M. Muksunov, A. S. Rupyshev, and V. V. Shapkin, "Interaction of stationary plasma with the materials of a thermonuclear reactor on model plants," VANT, Ser. Termoyad. Sintez, No. 4, 24–31 (2008).
8. A. Bernard, H. Bruzzone, P. Choi, H. Chuaqui, V. Gribkov, J. Herrera, K. Hirano, A. Krejci, S. Lee, C. Luo, F. Mezzetti, M. Sadowski, H. Schmidt, K. Ware, S. Wong, and V. Zoita, "Scientific status of plasma focus research," J. Moscow Phys. Soc. **8** (2), 93–170 (1998).
9. A. Cicuttin, M. L. Crespo, V. A. Gribkov, J. Niemela, C. Tuniz, C. Zanolli, M. Chernyshova, E. V. Demina, S. V. Latyshev, V. N. Pimenov, and A. A. Talab, "Experimental results on the irradiation of nuclear fusion relevant materials at the dense plasma focus "Bora" device," Nucl. Fusion **55**, 063037 (2015). https://doi.org/10.1088/0029-5515/55/6/063037
10. V. A. Gribkov, "Physical processes taking place in dense plasma focus devices at the interaction of hot plasma and fast ion streams with materials under test," Plasma Phys. Control. Fusion **57**, 065010 (2015). https://doi.org/10.1088/0741-3335/57/6/065010
11. V. A. Gribkov, L. Karpinski, P. Strzyzewski, M. Scholz, and A. V. Dubrovsky, "New efficient low-energy dense plasma focus in IPPLM," Czechoslovak J. Phys. **54** (Suppl.), 191–197 (2004).
12. S. A. Maslyaev, "Thermal effects during the pulsed irradiation of materials in a Plasma Focus plant," Perspekt. Mater., No. 5, 47–55 (2007).
13. G. G. Bondarenko, "Effect of irradiation on evaporation of several structural materials," Soviet Mater. Sci. **24** (5), 514–515 (1989).
14. V. N. Pimenov, V. A. Gribkov, L. I. Ivanov, M. Shol'ts, Yu. E. Ugaste, E. V. Demina, S. A. Maslyaev, A. V. Dubrovskii, R. Miklashevskii, B. Kolman, and A. A. Kadentsov, "On new possibilities of Plasma Focus plants for surface modification of materials," Perspekt. Mater., No. 1, 13–23 (2003).
15. E. V. Demina, L. I. Ivanov, S. A. Maslyaev, V. N. Pimenov, I. P. Sasinovskaya, V. A. Gribkov, and A. V. Du-

brovskii, "Surface modification of steel tubes by pulsed ion and high-temperature plasma fluxes," Perspekt. Mater., No. 5, 41–48 (2008).

16. I. V. Borovitskaya, V. Ya. Nikulin, G. G. Bondarenko, A. B. Mikhailova, P. V. Silin, A. I. Gaidar, V. V. Paramonova, and E. N. Peregudova, "Effect of pulsed nitrogen plasma and nitrogen ion fluxes on the structure and mechanical properties of vanadium," Russ. Metall. (Metally), No. 3, 266–275 (2018).
17. V. A. Gribkov, E. V. Demina, A. V. Dubrovskii, L. I. Ivanov, A. V. Kovtun, T. I. Laas, S. A. Maslyaev, V. N. Pimenov, A. Tartari, Yu. E. Ugaste, and M. Shol'ts, "Effect of pulsed fluxes of high-density deuterium and hydrogen plasma on ferritic and austenitic steels in a Plasma Focus plant," Perspekt. Mater., No. 1, 16–25 (2008).
18. S. V. Latyshev, V. A. Gribkov, S. A. Maslyaev, V. N. Pimenov, M. Padukh, and E. Zelin'ska, "Generation of shock waves in materials science experiments on a Plasma Focus plant," Perspekt. Mater., No. 8, 5–12 (2014).
19. I. V. Borovitskaya, V. N. Pimenov, V. A. Gribkov, M. Padukh, G. G. Bondarenko, A. I. Gaidar, V. V. Paramonova, and E. V. Morozov, "Structural changes in the vanadium sample surface induced by pulsed high-temperature deuterium plasma and deuterium ion fluxes," Russ. Metall. (Metally), No. 11, 928–935 (2017).
20. G. G. Bondarenko, Ya. Ya. Udris, N. V. Chikharev, and V. L. Yakushin, "Behavior of aluminum materials on irradiation by powerful pulsed hydrogen-plasma fluxes," Russ. Metall. (Metally), No. 3, 91–95 (1998).
21. I. I. Novikov, *Theory of Heat Treatment of Metals* (Metallurgiya, Moscow, 1986).

Translated by K. Shakhlevich